Journal of Colloid and Interface Science 469 (2016) 78–85

Contents lists available at ScienceDirect

Journal of Colloid and Interface Science

journal homepage: www.elsevier.com/locate/jcis

Catalytic reduction–adsorption for removal of p-nitrophenol and its conversion p-aminophenol from water by gold nanoparticles supported on oxidized mesoporous carbon

Pucan Guo, Lin Tang *, Jing Tang, Guangming Zeng *, Binbin Huang, Haoran Dong, Yi Zhang, Yaoyu Zhou, Yaocheng Deng, Linlin Ma, Shiru Tan

College of Environmental Science and Engineering, Hunan University, Changsha 410082, PR China
Key Laboratory of Environmental Biology and Pollution Control, Hunan University, Ministry of Education, Changsha 410082, PR China

GRAPHICAL ABSTRACT

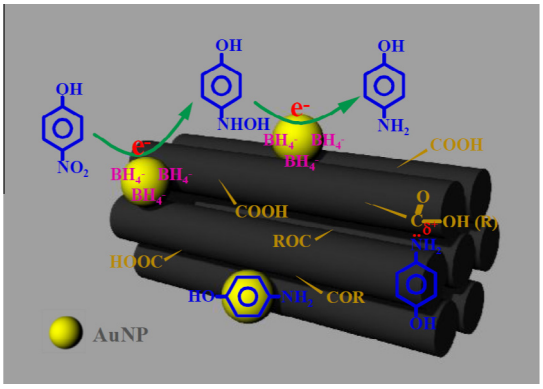

ARTICLE INFO

Article history:
Received 2 December 2015
Revised 27 January 2016
Accepted 27 January 2016
Available online 28 January 2016

Keywords:
Oxidized mesoporous carbon
Gold nanoparticles
Catalytic reduction–adsorption
p-Aminophenol
p-Nitrophenol

ABSTRACT

A highly efficient method for removal of p-nitrophenol and its conversion p-aminophenol from water was proposed using a novel catalyst–adsorbent composite of gold nanoparticles supported on functionalized mesoporous carbon (Au@CMK-3-O). The immobilized gold nanoparticles presented excellent catalytic ability to converse p-nitrophenol into p-aminophenol with the help of sodium borohydride, and the oxidized mesoporous carbon (CMK-3-O) serving as both carrier and adsorbent also exhibited high efficiency to remove p-aminophenol. The morphology and structure of the composite were characterized via SEM, TEM, FTIR and XPS analysis. Moreover, the mechanism of reaction process and the parameters of kinetics and thermodynamics were investigated. The activation energy was figured as 86.8 kJ mol^{-1} for the adsorption and reduction of p-nitrophenol to p-aminophenol. The thermodynamic analysis based on the rate constants evaluated by pseudo-first-order model reveals that the adsorption–reduction process is an endothermic procedure with the rise of randomness. The anti-oxidation and regeneration study indicates that Au@CMK-3-O can be reused for 6 times with more than 90% conversion efficiency and keep high activity after exposing in air for 1 month, which possesses great prospects in application of nitroaromatic pollutant removal.

* Corresponding authors at: College of Environmental Science and Engineering, Hunan University, Changsha 410082, PR China.
E-mail addresses: tanglin@hnu.edu.cn (L. Tang), zgming@hnu.edu.cn (G. Zeng).

http://dx.doi.org/10.1016/j.jcis.2016.01.063
0021-9797/

1. Introduction

Nitroaromatic compounds such as nitrophenol and nitrobenzene are important fundamental materials to produce pharmaceuticals, pesticides, explosives, dyes and other industrial chemicals [1]. Due to its toxicity and hazard, nitrophenol has been regarded as one of the priority pollutants by US Environmental Protection Agency (EPA) [2]. Many methods have been proposed to remove it from aquatic environment, such as adsorption, microbial degradation, and electrochemical treatment [3,4]. Nevertheless, the conventional treatment approaches have some major shortcomings. The slow degradation rate, limited degradation efficiency, secondary pollution, high costs and strict operating condition remarkably limit their wide applications in large scale [5–7]. Recently, hydrogenate reduction method caught researchers' eyes in the following aspects. On one hand, the generated aminophenol can serve as an important intermediate for cosmetic product, analgesics and antipyretics [8], which is a feasible way to convert pollutants such as nitrophenol to renewable resource. On the other hand, aminophenol is relatively less toxic and easier to be removed and mineralized compared to nitroaromatic compounds [9,10].

In the past few years, nanoscience and nanoparticles have been raising more attention in wastewater treatment process [11]. The nanoparticles have special physical and chemical properties, including large specific surface area, fine size and shape, high surface energy and Fermi potential, etc. [12]. With the use of noble nanoparticles (NNPs), a facile, green and cost-effective method for nitrophenol compounds reduction became reality. The conventional synthetic process is under a relatively high temperature and high hydrogen pressure in ethanol solvent [4]. The involved NNPs can serve as the electron relay between nitrophenol (oxidant) and BH_4^- (reductant), and the electron transfer occurs via the NNPs. Thus, such method is more environmental-friendly, cost-effective and energy-saving. Their operation condition is more safety and organic solvent-free as well, which are all key advantages over traditional ways [13]. These advantages make it possible to apply NNPs to treat industrial wastewater mainly containing nitrophenol compounds. But in practical use, the bare nanoparticles could inevitably bring about some problems. The nanomaterials can increase the potential risk of environment [14–16]. In addition, it is hard to separate them from the treatment system, and the particles are easy to aggregate [17,18]. Unlike bare NNPs, the immobilized NNPs show superior performance in unit operations. Some papers reported that NNPs supported on metal oxides, carbon materials or membrane exhibit fine diameter and well distribution, and is much easier for solid–liquid separation and recycle [19–21]. All of the immobilized NNPs manifest high transformation efficiency and rate of nitrophenol. Meanwhile, they could reduce the potential risks induced by nanoparticles as well [22]. Considering the supporter, ordered mesoporous carbon (OMC) is among the most proper materials as described below. First, the large surface area and special pore structure promote their access to disperse nanoparticles on the sites of OMC. Second, it's easy to be modified with functional groups during or after synthesis process. Third, the superior mechanical and thermal stabilities promise its use in practice [23,24].

In the present paper, a novel kind of composite, gold nanoparticles (AuNPs) which own less toxicity [25] anchored in oxidized OMC (CMK-3-O), was prepared. In catalytic activity test, Au@CMK-3-O exhibited high efficiency to transfer high concentration of p-nitrophenol (PNP) into p-aminophenol (PAP) rapidly in mild condition. Meanwhile, p-aminophenol is removed effectively via adsorption onto CMK-3-O supporters. The Au@CMK-3-O catalyst was characterized by TEM, XPS and FTIR. The mechanism of reaction process was revealed by XPS and GC–MS analysis. The stability and related kinetic and thermodynamic parameters were also explored.

2. Methods and material

2.1. Materials

Pluronic copolymer P123 (EO20PO70EO20, EO = ethylene oxide, PO = propylene oxide) was the production of Sigma–Aldrich (USA), and all other chemical regents used were of analytical grade except that dichloromethane was of chromatographic reagent grade. All stock solutions were prepared with high-purity water (18.25 MΩ cm, Milli-Q).

2.2. Preparation of CMK-3 and CMK-3-O carbon

The preparation of mesostructured SBA-15 hard silica template was in accord with described procedures of reported literature [26]. The synthesis of mesoporous carbon CMK-3 utilized SBA-15 silica template as pioneer. In specific, 1.25 g sucrose was dissolved into 5 mL aqueous solution containing 0.14 g H_2SO_4. Then, 1 g of calcined SBA-15 template was added into the mixed solution. The polymerization of mixture was conducted in an oven at 100 °C and then 160 °C for each 6 h. For the sake that polymerized sucrose was fully filled in the pores of the SBA-15 template, the pre-treated sample was immersed in 5 mL of multicomponent aqueous solution with 0.8 g sucrose and 0.09 g H_2SO_4, and the resulting mixture was heated again following thermal steps described above. For further carbonization, the resultant material was calcined in flowing nitrogen atmosphere at a heating rate of 5 °C min^{-1} to 900 °C for 6 h. Next, the materials was treated with 1 mol L^{-1} boiling solution of NaOH (50 vol% ethanol–50 vol% H_2O) several times to remove the silica template, followed by washing with 50% ethanol solution until pH = 7, and finally dried at 60 °C for 24 h [27]. At this point, the mesoporous carbon CMK-3 was obtained. To realize its functionalization, 0.2 g CMK-3 was diffused in 10 mL HNO_3 (10%) solution under refluxing at 110 °C for 1 h. Then, it was washed with deionized water until pH = 7, filter, dried at 90 °C for 12 h [28]. Thus, the oxidized mesoporous carbon CMK-3-O was attained.

2.3. Fabrication of Au@CMK-3-O

To immobilize AuNPs on the surface of CMK-3-O, incipient wetness impregnation technique was adopted. First, 0.1 g CMK-3-O was dispersed in 10 mL aqueous solution of 0.01 M $HAuCl_4$ at pH 4.0. Second, 25 mL reducing solvent of 0.1 M ascorbic acid was added into resulting solution drop by drop in N_2 atmosphere with vigorous stirring lasting for 25 min. The involved reaction was as followed.

$$2AuCl_4^- + 3C_6H_8O_6 == 2Au + 8Cl^- + 3C_6H_6O_6 + 6H^+ \quad (1)$$

Third, the product was washed by deionized water several times until pH = 7. Finally, it was dried overnight at 25 °C in a vacuum oven. Then the Au@CMK-3-O composite was obtained [29].

2.4. Apparatus and characterization

The surface morphologies of samples were analyzed by a Hitachi S4800 scanning electron microscope (SEM) and a JEM-3010 transmission electron microscopy (TEM) at 5.0 kV and 100 kV respectively. The surface area and distribution of pore size of products was obtained from a Quantachrome Nova 2200e instrument using BET and BJH method, respectively. The absorbance of

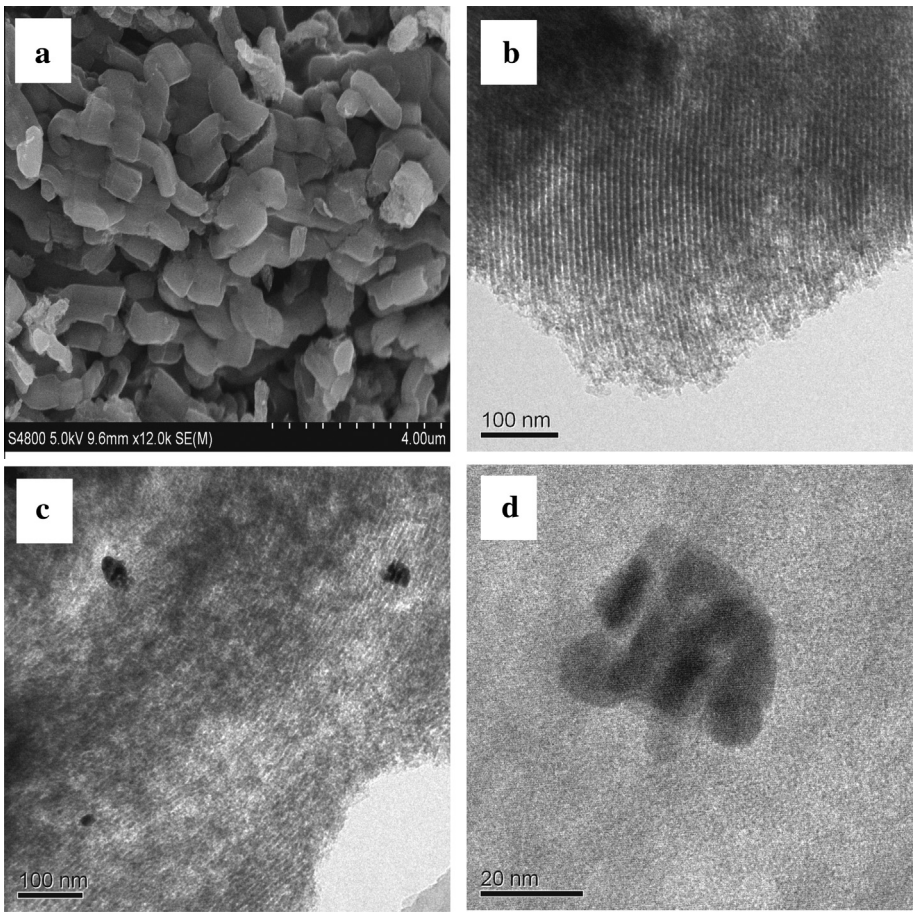

Fig. 1. SEM images of CMK-3-O (a) and TEM images of CMK-3-O (b) and Au@CMK-3-O (c, d).

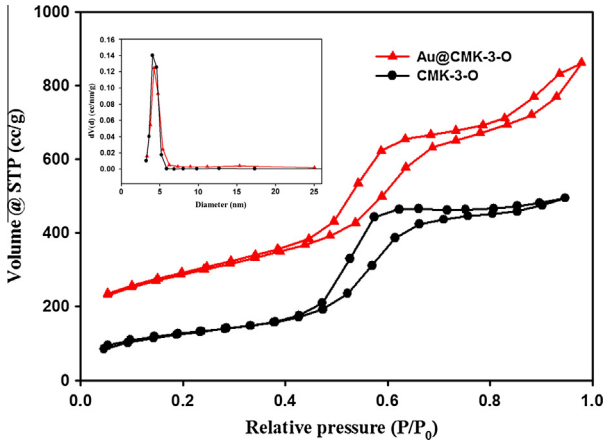

Fig. 2. Nitrogen adsorption–desorption isotherms and pore size distribution of CMK-3-O and Au@CMK-3-O.

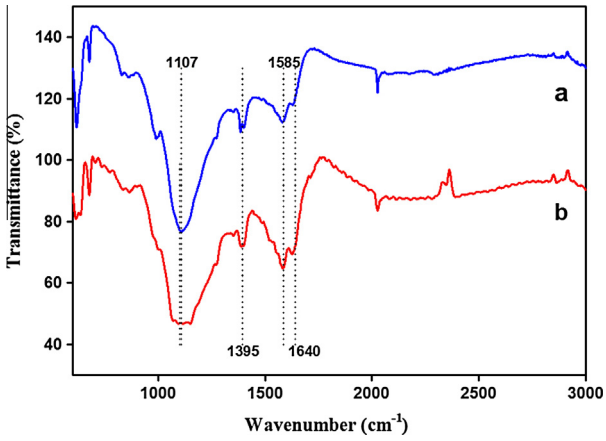

Fig. 3. FTIR spectra of CMK-3 (a) and Au@CMK-3-O (b).

PNP and PAP was verified by a SHIMADZU 2550 UV–Vis spectrophotometer. Fourier transform infrared (FTIR) spectra of the samples were recorded with an IRAffinity-1 FTIR spectrometer by the standard KBr disk method. The surface chemical composition of Au@CMK-3-O materials was investigated by a Thermo Fisher Scientific X-ray photoelectron spectroscopy (XPS) before and after interaction. The QP2010-PLUSGC/MS system (SHIMADZU, Japan) attached with a HP-5MS capillary column was utilized to qualitatively identify intermediate products of PNP during interaction.

2.5. Reaction studies

The study of catalytic reduction of PNP and adsorption of PAP was carried out in 250 mL conical flask at 150 rpm rate. In detail, 75 mg Au@CMK-3-O materials or CMK-3-O carrier was dispersed in multi-component solution including 0.06 M $NaBH_4$ and 200 mg/L PNP. In theory, 200 mg/L PNP can be transferred into no more than 156.9 mg/L PAP, so the adsorption test about PAP was the same as the catalytic study mentioned above in which the initial concentration of PAP is expected to be 156.9 mg/L. To assess the adsorption

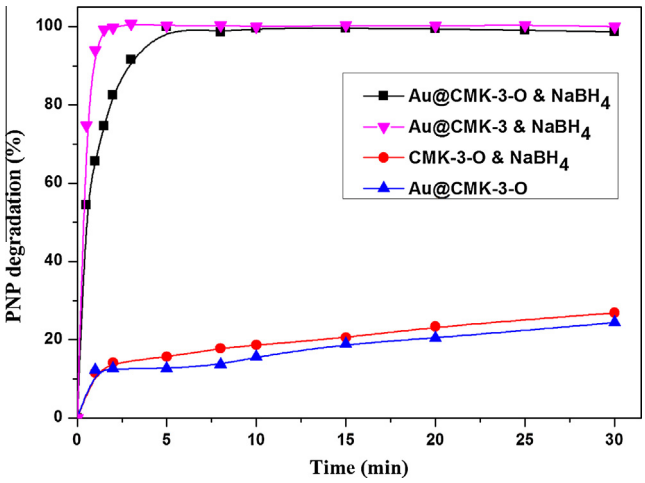

Fig. 4. Removal efficiency of 200 mg/L PNP by CMK-3-O, Au@CMK-3 and Au@CMK-3-O at 25 °C.

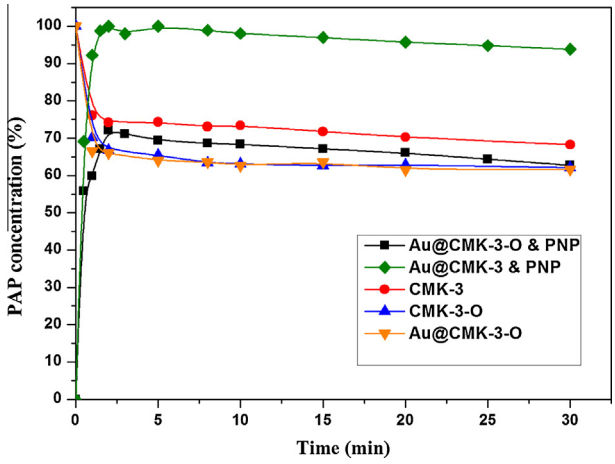

Fig. 5. Relative concentration of PAP vs. time in the systems containing 156.9 mg/L PAP and CMK-3, CMK-3-O, Au@CMK-3 or Au@CMK-3-O, and in the solution containing 200 mg/L PNP and Au@CMK-3-O with 0.06 M $NaBH_4$ at 25 °C.

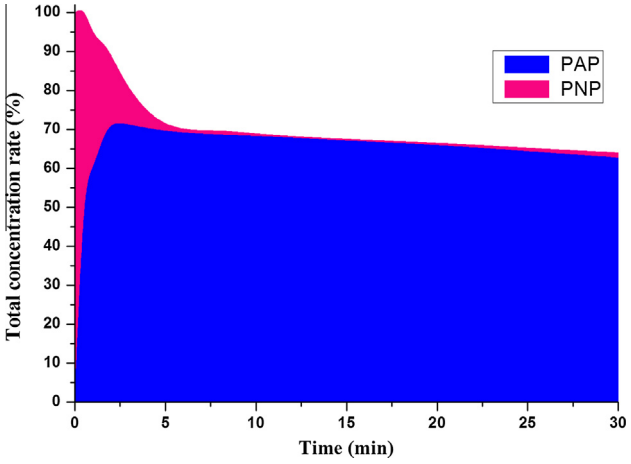

Fig. 6. Total degradation by Au@CMK-3-O in reduction system with the initial PNP concentration of 200 mg/L at 25 °C.

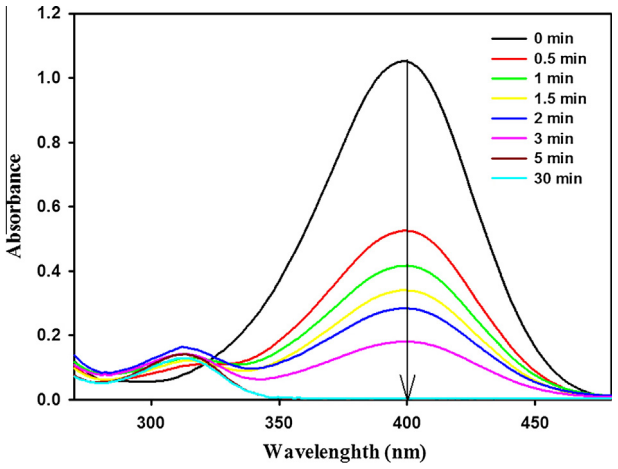

Fig. 7. UV–Vis spectra of the reduction of PNP by Au@CMK-3-O.

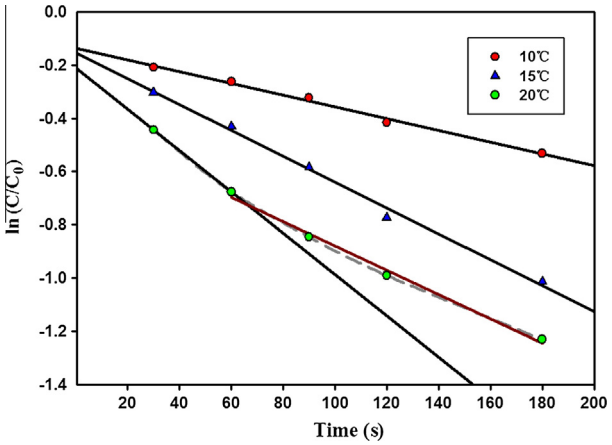

Fig. 8. The pseudo-first-order kinetic plot for the adsorption-catalytic reduction of PNP at different temperature.

contribution of Au@CMK-3-O composite during process of PNP removal, 75 mg Au@CMK-3-O catalyst was added into solution of 200 mg/L PNP at pH 10.15 because the pH value of such reduction system maintained approximately at 10.15. The residual concentration of PNP was monitored at a wavelength of 400 nm after alkalizing by NaOH [30]. Treated by method of Berthlot, the concentration of PAP was determined at a wavelength of 632 nm [31].

The degradation efficiencies were calculated according to the following equations:

$$R(\%) = \frac{C_0 - C_1}{C_0} \times 100 \quad (2)$$

$$q(\%) = \frac{C_1}{C_0} \times 100 \quad (3)$$

where C_0 and C_1 are the initial and residual concentration of aqueous PNP (mg/L) or PAP (mg/L), respectively; $R(\%)$ is the conversion efficiency and $q(\%)$ is the relative concentration ratio of residues.

The reuse and anti-oxidation studies of Au@CMK-3-O were carried out in the batch experiments. Typically, the Au@CMK-3-O exposed in air for 0 or 30 days suspended in multicomponent solution in the same condition as described above. The used Au@CMK-3-O was filtered from the suspension and then washed with ultrapure water for twice. After separation and dried overnight at 25 °C in a vacuum oven, the regenerative catalyst was collected for next cycle.

Table 1
Kinetic and thermodynamic parameters for the catalytic reduction of PNP.

T (K)	k (min^{-1})	r^2	E_a (kJ mol^{-1})	r^2_A	$\Delta H^{\#}$ (kJ mol^{-1})	$\Delta S^{\#}$ (J mol^{-1} K^{-1})	r^2_e
283	0.132	0.993	86.8	0.981	84.4	686	0.980
288	0.292	0.994					
293	0.465	–					
	0.274	0.993					

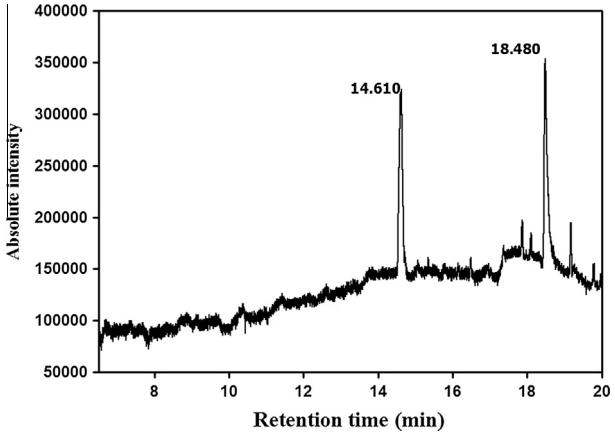

Fig. 9. GC–MS chromatograms on dichloromethane extract from the treatment effluent of Au@CMK-3-O.

GC/MS analysis was developed after a series of pre-treatment [32,33]. In specific, a 50 mL sample was extracted with 10 mL dichloromethane three times under acidic (pH ≈ 2.0), neutral (pH ≈ 7.0) and alkaline (pH ≈ 12.0) conditions, respectively. The three extracted layers were mixed together, and then using extra anhydrous sodium sulfate to dewater. With intensive nitrogen stream, the mixture was dried in ambient temperature. The residue was dissolved in 1.0 mL CH_2Cl_2 and 1 μL of the solution was injected into the GC/MS system. The GC column ran in a temperature program mode starting at 40 °C for 3 min, rising up to 280 °C in speed of 10 °C min^{-1}, and keeping at 280 °C for 5 min. The solvent delay was 6 min, and the total run time was 32 min. The mass range scanned was 20–500 *m*/*z*. The qualitative analysis of conversion products was based on the mass spectral library database.

3. Results and discussion

3.1. Characterization of Au@CMK-3-O

The morphological properties of CMK-3-O and Au@CMK-3-O were characterized by TEM and SEM techniques (Fig. 1). The images in Fig. 1a and b show that the carrier CMK-3-O has rod-like shape with well-ordered linear array of mesoporous structures. Fig. 1c and d show the TEM images of Au@CMK-3-O with different resolutions. It reveals that black spherical AuNPs have been distributed on the surface of CMK-3-O matrix, but a slight agglomeration can still be observed, which is because the surface of CMK-3-O has been partly oxidized. And the diameter of AuNPs is approximate 10 nm. The textural properties were offered by the nitrogen adsorption–desorption test. The isotherm curves (Fig. 2) shows that two hysteresis loops are in harmony with typical type IV curves with featured capillary condensation at the relative pressure (P/P_0) of 0.5–0.8, indicating few structure changes of CMK-3-O after AuNPs anchored and the presence of well uniform mesopores in two samples, which is further convinced by the pore diameter distribution curves. The BET and BJH analysis indicates that after immobilizing AuNPs on the CMK-3-O matrix, the surface area of CMK-3-O decreased from 1101.04 m^2/g to 984.56 m^2/g, the diameter of pore size dropped from 4.77 nm to 4.25 nm, and the pore volume reduced from 1.27 cm^3/g to 1.19 cm^3/g. This might relate to that immobilized AuNPs occupied the surface sites and block some parts of pores.

The FTIR spectra of CMK-3 and Au@CMK-3-O are recorded in Fig. 3, and they show the main chemical structure of samples. The absorption peak around 1107 cm^{-1} reveals C—O stretching vibrations from oxygen groups. The bands appearing at 1395 cm^{-1} corresponds to C—H bending vibrations in —CH_2 and —CH_3 groups. Moreover, the strong bands at 1585 cm^{-1} is attributed to —COO^- asymmetric vibrations and C=C stretching vibrations. The weak bands at 1640 cm^{-1} is indicated by C=O stretching vibrations [27,28,34]. The characteristic peak at 2027 cm^{-1} is not observed in CMK-3-O structure reported before, which is related to C≡C in-line deformation vibrations. In comparison with such two spectra of samples, it is obvious to notice that the peaks at 1585 cm^{-1} and 1640 cm^{-1} of spectra (b) are deeper, which reveals that the surface of CMK-3 was modified with carbonyl group and carboxyl group successfully after functionalization by nitric acid.

3.2. Catalysis reduction and adsorption process of PNP

The coupling of catalysis-adsorption to degrade PNP is presented in Fig. 4. It illustrates that due to the decrease of the surface area after immobilization of AuNPs, the adsorption capacity is slightly reduced. And within 5 min, 200 mg/L PNP aqueous pollutant was removed totally. As time went by, the contribution of catalytic reduction increased from 53% at 1 min to 87% at 5 min, which indicates that the anchored AuNPs indeed have excellent catalytic activity to the conversion of PNP. Interestingly, Au@CMK-3 performed higher rate for PNP removal given that CMK-3 are more beneficial to AuNPs load and dispersion, however, its PAP removal capacity was negligible. The PAP removal process was observed within 30 min (Fig. 5). It reflects that CMK-3-O has an apparent advantage to adsorb PAP pollutant over CMK-3. But CMK-3-O and Au@CMK-3-O materials don't make too much difference in terms of PAP adsorption, this is because low loaded AuNPs don't occupy surface sites for catching PAP. In addition, in catalytic reduction system, the equilibrium concentration of PAP is nearly the same as the results of those in adsorption test with initial PAP concentration of 156.9 mg/L. And this indicates that PNP has been transferred into PAP thoroughly. Fig. 6 refers to the total capacity for the removal of such two compounds. The ability to remove PNP is much higher than that for PAP for it is only wiped off through adsorption process. The same trend is also observed in Fig. 7. The characteristic peak of PNP shifted from 317 nm to 400 nm in extreme alkalinity, generating p-nitrophenolate ions, and its intensity of absorbance can stay for 2 days. Fig. 6 shows that the peak at 400 nm decreases sharply while a small peak appears at 310 nm and keeps up with slight weakening, which refers to the residual product of p-aminophenolate ions [35].

3.3. Kinetic and thermodynamic studies

The kinetic and thermodynamic parameters of the catalytic reduction of PNP are important as far as industrial waste water

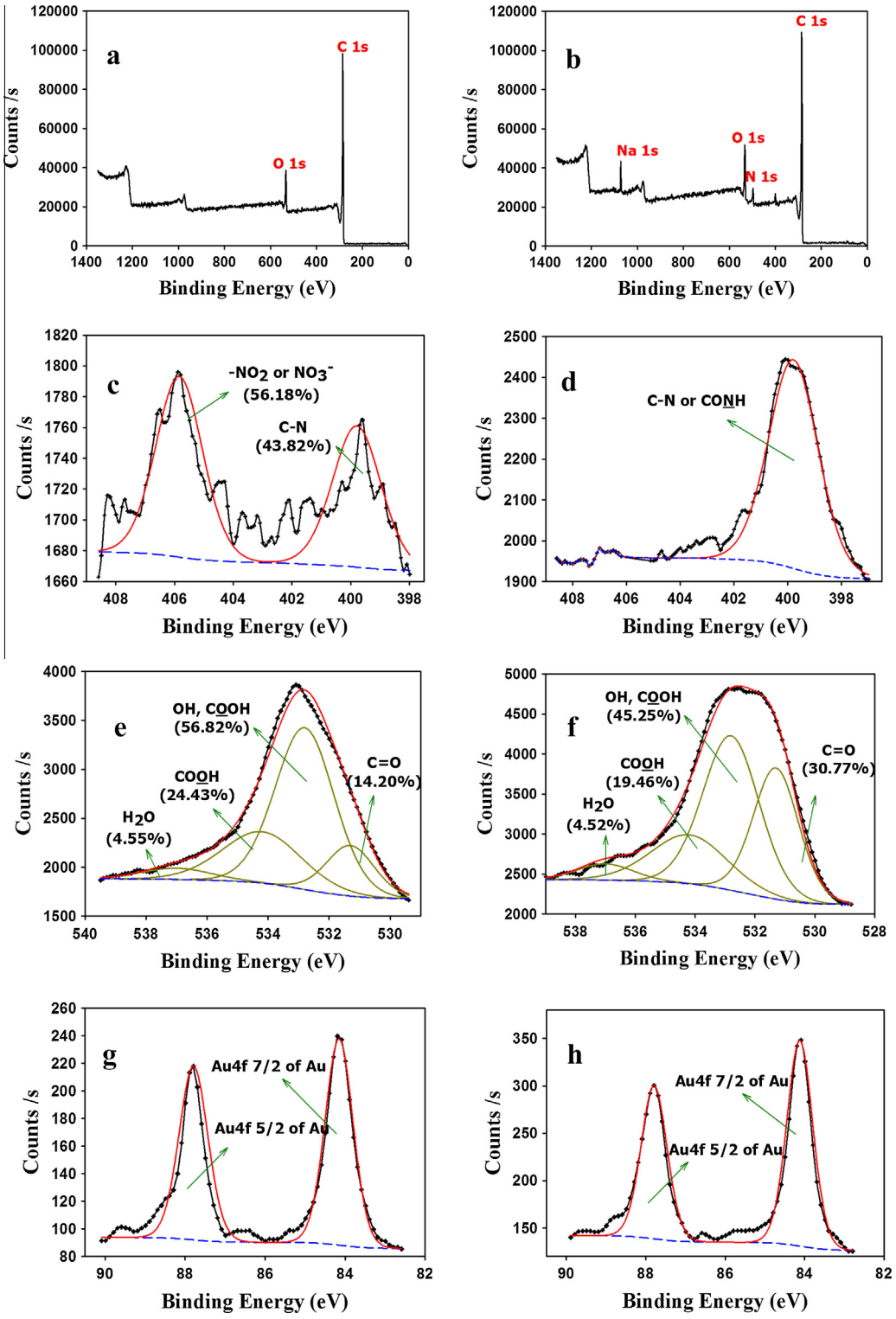

Fig. 10. XPS spectra of Au@CMK-3-O before (a, c, e, g) and after (b, d, f, h) reduction.

treatment concerned. The reaction rate constants (k) are calculated according to pseudo-first-order kinetic model. The plots of $\ln C/C_0$ versus time (Fig. 8) at 10 °C and 15 °C manifest good linear correlation to the kinetic model, while the plot at 20 °C can be divided into two steps. At the beginning, the concentrate of PNP dropped quickly due to the bifunction of catalytic reduction and adsorption. Then, the value of reaction rate constant apparently decreased, which might be owed to that the rising temperature caused the higher adsorption rate but lower adsorption capacity, and hence hydrogenated reduction dominated the process while adsorption failed to act. The values of reaction rate constant and correlation coefficients are listed in Table 1. The Arrhenius activation energy of catalytic reduction–adsorption step was determined using following equation (4):

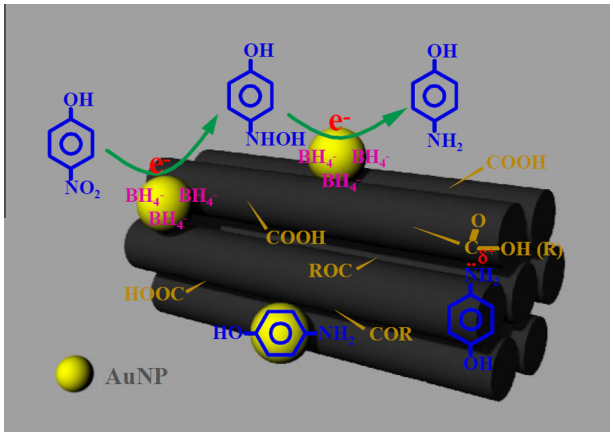

Scheme 1. A possible pathway for the removal of PNP and PAP compounds by Au@CMK-3-O in $NaBH_4$ reduction system.

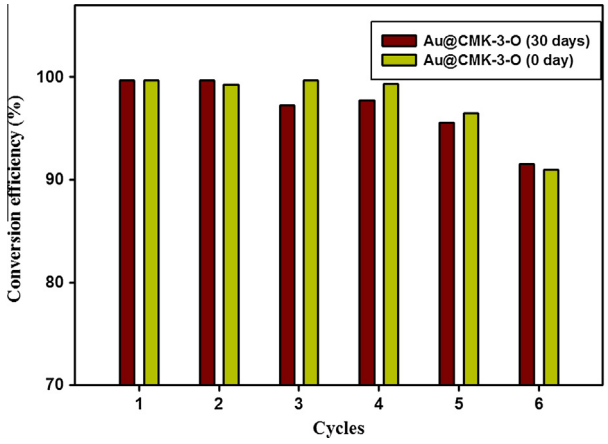

Fig. 11. Degradation of PNP using Au@CMK-3-O materials for 6 cycles with initial PNP concentration of 200 mg/L.

$$\ln k = \ln A - \frac{E_a}{RT} \tag{4}$$

where E_a is activation energy, A is pre-exponential factor (or simply the prefactor), and R is the universal gas constant. The value of E_a is figured out from the slope of linear plot of $\ln k$ versus $1/T$. The value of activation energy is 86.8 kJ mol^{-1}, and it reveals that the surface interaction of eliminating PNP has low energy barrier.

The thermodynamic parameters such as enthalpy change ($\Delta H^{\#}$) and entropy change ($\Delta S^{\#}$) are acquired with Eq. (5), Eyring equation:

$$\ln\frac{k}{T} = \ln\frac{k_B}{T} + \frac{\Delta S^{\#}}{R} - \frac{\Delta H^{\#}}{R}\left(\frac{1}{T}\right) \tag{5}$$

where k_B is Boltzmann constant. The thermodynamic parameters are attained with plots of $\ln k/T$ against $1/T$ where the slope of straight line is $-\Delta H^{\#}/R$. The values of activation energy and related thermodynamic parameters with their correlation coefficient are listed in Table 1. As we can see, the thermodynamic parameters illustrate an endothermic procedure with the rise of randomness during PNP removal process.

3.4. Interaction mechanism

To determine a possible pathway for the reduction of PNP, gas chromatography–mass spectrometry (GC/MS) was used to detect various intermediates. As shown in Fig. 9, the peaks occurring at 14.610 min and 18.480 min refer to the PAP and PNP compounds with 91% and 88% similarities, respectively. No by-product is found out, which indicates this catalytic reduction is highly specific to convert PNP into PAP.

The XPS technique was applied to determine the surface chemical structure changes of Au@CMK-3-O materials before and after interaction (Fig. 10). The spectrums of surveys are proposed in Fig. 10a and b. As expected, the peaks of carbon (C1s) and oxygen (O1s) can been seen clearly, and after reaction, two new peaks about nitrogen (N1s) and sodium (Na1s) turn up in the spectrum (Fig. 10b), which is related with the adhesion of sodium ions and PAP compounds. Before PAP uptake, N1s core level spectrum (Fig. 10c) shows two distinct peaks at 405.8 and 399.8 eV, which correspond to the residual nitrate ions or nitro group and C—N structures, respectively. But after adsorption of PAP compounds, the peak at 405.8 eV is so weak that cannot be detected while the peak at 399.8 eV is clear to be observed (Fig. 10d). This suggests that electron withdrawing groups, like —COOH and C=O groups, caught the —NH_2 of PAP, and —CO—NH— bond was generated, accelerating the extermination of PAP compounds. The O1s region were fitted with four peaks at 531.3 eV (C=O in quinone), 532.8 eV (oxygen in hydroxyl, carboxyl (OH, COOH) as well as nitro group bonded to aromatic ring (N—O)), 534.2 eV (hydroxyl in carboxyl group (COOH)) and 537.0 eV (adsorbed water) [34]. From Fig. 10e and f, it is evident to notice that the peak at 531.3 eV was increased from 14.20% to 30.77%. This can be attributed to that PAP compounds were oxidized by air and converted to 4-benzoquinone [33], which also indirectly confirms that PAP compounds attached on the surface of Au@CMK-3-O materials. The spectra of Au4f (Fig. 10g and h) consist of two spectral lines about Au4f 7/2 and Au4f 5/2 of AuNPs with 84.1 eV and 87.8 eV binding energy. Fig. 10g was very similar to Fig. 10h, and this hints the AuNPs work as catalyst in reduction system without chemical form changes.

Considering the mechanism studies mentioned above, a possible mechanism for the reduction of PNP was proposed (Scheme 1) [29,36,37]. The heterogeneous reaction can be divided into four steps: (i) adsorption of PNP to Au@CMK-3-O materials, (ii) diffusion of PNP to active sites on AuNPs, (iii) catalytic reduction of PNP to PAP with a 6 electrons-transmission process between PNP and $NaBH_4$, (iv) PNP release and PAP uptake onto the CMK-3-O surface site.

3.5. Ability of anti-oxidation and regeneration studies of Au@CMK-3-O

Fig. 11 shows the PNP conversion efficiency of two samples after 6 cycles. As it indicates, the Au@CMK-3-O materials exposed in air for 30 days did not manifest overt distinction compared with those freshly made. That reveals Au@CMK-3-O materials have perfect properties against oxygen corrosion. The regeneration study indicates that Au@CMK-3-O can be reused for 6 times with more than 90% conversion efficiency. To sum up, Au@CMK-3-O materials have excellent stable abilities without losing many active sites after being exposed in air or reused for at least 6 times.

4. Conclusion

In summary, a novel Au@CMK-3-O composite material was fabricated and comprehensively characterized. By using the preparation approach with HNO_3, the CMK-3 surface was successfully oxidized, and AuNPs were loaded with a diameter of 10 nm. In PNP removal tests, Au@CMK-3-O exhibited high performance in removing PNP. The conversion efficiency could reach 100% within only 5 min, and no by-products were generated. In further removal process, Au@CMK-3-O provided better PAP adsorption capacity

than CMK-3 and Au@CMK-3. This could be ascribed to the abundant carbonyl/carboxyl groups on large surface area, significantly promoting the uptake of PAP. Moreover, the reaction kinetics results indicated that the novel material showed lower energy barrier in eliminating PNP compounds. The thermodynamic parameters revealed that PNP catalysis-adsorption process is an endothermic procedure with the rise of randomness. The stability tests confirmed that Au@CMK-3-O remained stable after being exposed in air and cycled for 6 times. The study provided an insight into the PNP removal via bifunction of hydrogenated reduction and adsorption, and might offer an easy and effective method to treat PNP-contaminated wastewater in industrial application.

Acknowledgments

The study was financially supported by the National Program for Support of Top–Notch Young Professionals of China (2012), Projects 51222805, 51579096 and 51521006 supported by National Natural Science Foundation of China, the Program for New Century Excellent Talents in University from the Ministry of Education of China (NCET-11-0129), the Fundamental Research Funds for the Central Universities, Hunan University.

References

[1] R. Emmanuel, C. Karuppiah, S.M. Chen, S. Palanisamy, S. Padmavathy, P. Prakash, Green synthesis of gold nanoparticles for trace level detection of a hazardous pollutant (nitrobenzene) causing Methemoglobinaemia, J. Hazard. Mater. 279 (2014) 117–124.
[2] J.H. Li, D.Z. Kuang, Y. L Feng, F.X. Zhang, Z.F. Xu, M.Q. Liu, A graphene oxide-based electrochemical sensor for sensitive determination of 4-nitrophenol, J. Hazard. Mater. 201–202 (2012) 250–259.
[3] J.R. Chiou, B.H. Lai, K.C. Hsu, D.H. Chen, One-pot green synthesis of silver/iron oxide composite nanoparticles for 4-nitrophenol reduction, J. Hazard. Mater. 248–249 (2013) 394–400.
[4] Y.C. Chang, D.H. Chen, Catalytic reduction of 4-nitrophenol by magnetically recoverable Au nanocatalyst, J. Hazard. Mater. 165 (2009) 664–669.
[5] Z. Liu, F. Cui, H. Ma, Z. Fan, Z. Zhao, Z. Hou, D. Liu, Bio-reaction of nitrobenzene with *Microcystis aeruginosa*: characteristics, kinetics and application, Water Res. 46 (2012) 2290–2298.
[6] J. Huang, Y. Wen, N. Ding, Y. Xu, Q. Zhou, Effect of sulfate on anaerobic reduction of nitrobenzene with acetate or propionate as an electron donor, Water Res. 46 (2012) 4361–4370.
[7] P. Roy, A.P. Periasamy, C.T. Liang, H.T. Chang, Synthesis of graphene–ZnO–Au nanocomposites for efficient photocatalytic reduction of nitrobenzene, Environ. Sci. Technol. 47 (2013) 6688–6695.
[8] J. Sun, Y. Fu, G. He, X. Sun, X. Wang, Catalytic hydrogenation of nitrophenols and nitrotoluenes over a palladium/grapheme nanocomposite, Catal. Sci. Technol. 4 (2014) 1742–1748.
[9] A.J. Wang, H.Y. Cheng, B. Liang, N.Q. Ren, D. Cui, N. Lin, B.H. Kim, K. Rabaey, Efficient reduction of nitrobenzene to aniline with a biocatalyzed cathode, Environ. Sci. Technol. 45 (2011) 10186–10193.
[10] J.Y. Shen, X.P. Xu, X.B. Jiang, C.X. Hua, L.B. Zhang, X.Y. Sun, J.S. Li, Y. Mu, L.J. Wang, Coupling of a bioelectrochemical system for p-nitrophenol removal in an upflow anaerobic sludge blanket reactor, Water Res. 67 (2014) 11–18.
[11] C.B. Wang, W.X. Zhang, Synthesizing nanoscale iron particles for rapid and complete dechlorination of TCE and PCBs, Environ. Sci. Technol. 31 (7) (1997) 2154–2156.
[12] N. Muniyappan, N.S. Nagarajan, Green synthesis of gold nanoparticles using Curcuma pseudomontana essential oil, its biological activity and cytotoxicity against human ductal breast carcinoma cells T47D, J. Environ. Chem. Eng. 2 (2014) 2037–2044.
[13] J. Xia, G. He, L. Zhang, X. Sun, X. Wang, Hydrogenation of nitrophenols catalyzed by carbon black-supported nickel nanoparticles under mild conditions, Appl. Catal., B: Environ. 408 (2016) 408–415.
[14] L. Fontanaa, V. Lesoa, A. Marinacciob, G. Cenacchic, V. Papac, K. Leopoldd, R. Schindld, B. Boccae, A. Alimontie, I. Iavicolia, The effects of palladium nanoparticles on the renal function of female Wistar rats, Nanotoxicology 9 (2015) 843–851.
[15] T. Leonardo, E. Farhi, S. Pouget, S. Motellier, A.M. Boisson, D. Banerjee, F. Rébeillé, C. Auwer, C. Rivasseau, Silver accumulation in the green microalga *Coccomyxa actinabiotis*: toxicity, in situ speciation, and localization investigated using synchrotron XAS, XRD, and TEM, Environ. Sci. Technol. 50 (2016) 359–367.
[16] M. Hashimoto, K. Kawai, H. Kawakami, S. Imazato, Matrix metalloproteases inhibition and biocompatibility of gold and platinum nanoparticles, J. Biomed. Mater. Res., Part A 104 (2016) 209–217.
[17] M. Wojnicki, M.L. Błocho, J. Grzonka, K. Pacławski, K.J. Kurzydłowski, K. Fitzner, Micro-continuous flow synthesis of gold nanoparticles and integrated deposition on suspended sheets of graphene oxide, Chem. Eng. J. 225 (2013) 597–606.
[18] H. Koga, T. Kitaoka, One-step synthesis of gold nanocatalysts on a microstructured paper matrix for the reduction of 4-nitrophenol, Chem. Eng. J. 168 (2011) 420–425.
[19] F.H. Lin, R.A. Doong, Bifunctional Au–Fe_3O_4 heterostructures for magnetically recyclable catalysis of nitrophenol reduction, J. Phys. Chem. C 115 (2011) 6591–6598.
[20] K. Pacawski, M. Wojnicki, Kinetics of the adsorption of gold (III) chloride complex ions onto activated carbon, Arch. Metall. Mater. 54 (2009) 560–853.
[21] R. Chen, Y. Jiang, W. Xing, W. Jin, Fabrication and catalytic properties of palladium nanoparticles deposited on a silanized asymmetric ceramic support, Ind. Eng. Chem. Res. 50 (2011) 4405–4411.
[22] L. Zhou, T.L. Thanh, J. Gong, J.-H. Kim, E.-J. Kim, Y.-S. Chang, Carboxymethyl cellulose coating decreases toxicity and oxidizing capacity of nanoscale zerovalent iron, Chemosphere 104 (2014) 155–161.
[23] Z.H. Xue, F. Zhang, D.D. Qin, Y.L. Wang, J.X. Zhang, J. Liu, Y.J. Feng, X.Q. Lu, One-pot synthesis of silver nanoparticle catalysts supported on N-doped ordered mesoporous carbon and application in the detection of nitrobenzene, Carbon 69 (2014) 481–489.
[24] G.D. Yang, L. Tang, Y. Cai, G.M. Zeng, P.C. Guo, G.Q. Chen, Y.Y. Zhou, J. Tang, J. Chen, W.P. Xiong, Effective removal of Cr(VI) through adsorption and reduction by magnetic mesoporous carbon incorporated with polyaniline, RSC Adv. 4 (2014) 58362–58371.
[25] M. Staszek, J. Siegel, S. Rimpelová, O. Lyutakov, V. Švorčík, Cytotoxicity of noble metal nanoparticles sputtered into glycerol, Mater. Lett. 158 (2015) 351–354.
[26] D. Zhao, Q. Huo, J. Feng, B.F. Chmelka, G.D. Stucky, Nonionic triblock and star diblock copolymer and oligomeric surfactant syntheses of highly ordered, hydrothermally stable, mesoporous silica structures, J. Am. Chem. Soc. 120 (1998) 6024–6036.
[27] L. Tang, G.D. Yang, G.M. Zeng, Y. Cai, S.S. Li, Y.Y. Zhou, Y. Pang, Y.Y. Liu, Y. Zhang, B. Luna, Synergistic effect of iron doped ordered mesoporous carbon on adsorption-coupled reduction of hexavalent chromium and the relative mechanism study, Chem. Eng. J. 239 (2014) 114–122.
[28] M. Baikousi, A.B. Bourlinos, A. Douvalis, T. Bakas, D.F. Anagnostopoulos, J. Tuček, K. Šafářová, R. Zboril, Michael A. Karakassides, Synthesis and characterization of γ-Fe_2O_3/carbon hybrids and their application in removal of hexavalent chromium ions from aqueous solutions, Langmuir 28 (2012) 3918–3930.
[29] V.K. Gupta, N. Atar, M.L. Yola, Z. Üstündağ, L. Uzun, A novel magnetic Fe@Au core–shell nanoparticles anchored graphene oxide recyclable nanocatalyst for the reduction of nitrophenol compounds, Water Res. 48 (2014) 210–217.
[30] S.X. Li, F.Y. Zheng, W.L. Cai, A.Q. Han, Y.K. Xie, Surface modification of nanometer size TiO_2 with salicylic acid for photocatalytic degradation of 4-nitrophenol, J. Hazard. Mater. 135 (2006) 431–436.
[31] T.T. Ngo, A.P.H. Phan, C.F. Yam, H.M. Lenhoff, Interference in determination of ammonia with the hypochlorite-alkaline phenol method of Berthelot, Anal. Chem. 54 (1982) 46–49.
[32] B. Lai, Y.H. Zhang, Z.Y. Chen, P. Yang, Y.X. Zhou, J.L. Wang, Removal of p-nitrophenol (PNP) in aqueous solution by the micron-scale iron–copper (Fe/Cu) bimetallic particles, Appl. Catal., B: Environ. 144 (2014) 816–830.
[33] L. Tang, J. Tang, G.M. Zeng, G.D. Yang, X. Xie, Y.Y. Zhou, Y. Pang, Y. Fang, J.J. Wang, W.P. Xiong, Rapid reductive degradation of aqueous p-nitrophenol using nanoscale zero-valent iron particles immobilized on mesoporous silica with enhanced antioxidation effect, Appl. Surf. Sci. 333 (2015) 220–228.
[34] P. Janus, R. Janus, P. Kuśtrowski, S. Jarczewski, A. Wach, A.M.S. Albero, F.R. Reinoso, Chemically activated poly(furfuryl alcohol)-derived CMK-3 carbon catalysts for the oxidative dehydrogenation of ethylbenzene, Catal. Today 235 (2014) 201–209.
[35] W. Zhang, F.T. Tan, W. Wang, X.L. Qiu, X.L. Qiao, J.G. Chen, Facile, template-free synthesis of silver nanodendrites with high catalytic activity for the reduction of p-nitrophenol, J. Hazard. Mater. 217–218 (2012) 36–42.
[36] S. Fountoulaki, V. Daikopoulou, P.L. Gkizis, I. Tamiolakis, G.S. Armatas, I.N. Lykakis, Mechanistic studies of the reduction of nitroarenes by $NaBH_4$ or hydrosilanes catalyzed by supported gold nanoparticles, ACS Catal. 4 (2014) 3504–3511.
[37] S. Gu, S. Wunder, Y. Lu, M. Ballauff, Kinetic analysis of the catalytic reduction of 4-nitrophenol by metallic nanoparticles, J. Phys. Chem. C 118 (2014) 18618–18625.